J. Fluid Mech. (2016), *vol.* 786, *pp.* 47–61.
doi:10.1017/jfm.2015.641

Universality of finger growth in two-dimensional Rayleigh–Taylor and Richtmyer–Meshkov instabilities with all density ratios

Qiang Zhang[1,†] **and Wenxuan Guo**[1]

[1]Department of Mathematics, City University of Hong Kong, 83 Tat Chee Avenue, Kowloon, Hong Kong

(Received 10 March 2015; revised 1 September 2015; accepted 28 October 2015;
first published online 25 November 2015)

Interfacial fluid mixing driven by an external acceleration or a shock wave are common phenomena known as Rayleigh–Taylor instability and Richtmyer–Meshkov instability, respectively. The most significant feature of these instabilities is the penetrations of heavy (light) fluid into light (heavy) fluid known as spikes (bubbles). The study of the growth rate of these fingers is a classical problem in fundamental science and has important applications. Research on this topic has been very active over the past half-century. In contrast to the well-known phenomena that spikes and bubbles can have quantitatively, even qualitatively, different behaviours, we report a surprising result for fingers in a two-dimensional system: in terms of scaled dimensionless variables, all spikes and bubbles at any density ratio closely follow a universal curve, up through a pre-asymptotic stage. Such universality holds not only among bubbles and among spikes of different density ratios, but also between bubbles and spikes of different density ratios. The data from numerical simulations show good agreement with our theoretical predictions.

Key words: fingering instability, interfacial flows (free surface), multiphase flow

1. Introduction

Interfacial fluid mixing is a common phenomenon that occurs frequently in basic science research and in engineering applications. Very often, the involved interface is unstable and small disturbances at the interface grow to form nonlinear structures. Particularly, the instabilities of the interface between two immiscible fluids, induced by an external force or a shock wave, have been intensively studied due to their essential role in understanding supernova explosions, inertial confinement fusion, etc. The former instability is known as Rayleigh–Taylor (RT) instability (Rayleigh 1883; Taylor 1950), and the latter one is known as Richtmyer–Meshkov (RM) instability (Richtmyer 1960; Meshkov 1969). The nonlinear structures at the unstable interface are known as spikes for the portion of heavy fluid penetrating into light fluid, and known as bubbles for the portion of light fluid penetrating into heavy fluid. To predict the growth rate of spikes and bubbles is very important for understanding the dynamics of unstable interfaces.

† Email address for correspondence: mazq@cityu.edu.hk

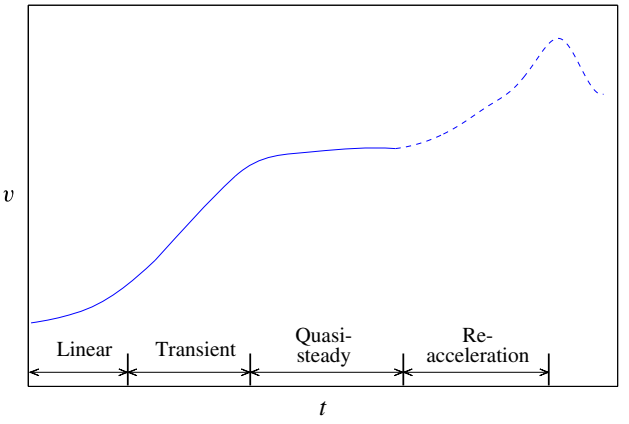

FIGURE 1. (Colour online) Sketch of different growth stages in RT instability, based on the numerical result from Glimm *et al.* (2002).

The studies of RT and RM instabilities have a long history. General reviews on RT and RM instabilities can be found in Sharp (1984) and Brouillette (2002). The results for RT and RM instabilities in incompressible, irrotational and inviscid systems can be traced from Hecht, Alon & Shvarts (1994), Zhang (1998), Glimm, Li & Lin (2002), Goncharov (2002), Abarzhi, Glimm & Lin (2003), Mikaelian (2003) and Sohn (2003, 2004). Many studies have showed that the development of RT instability starts with a linear stage, and transits into a quasi-steady stage at late times. In the quasi-steady stage, the growth rates of the fingers are insensitive to time for systems with finite density ratios (see the solid curve in figure 1). Since most of the previous experiments, numerical simulations and theoretical studies were performed up through the quasi-steady stage, we will focus on the development of the instability in the quasi-steady stage. New numerical studies (Glimm *et al.* 2002; Sohn 2011) on RT instability suggested that, beyond this stage, the growth rate may experience a period of re-acceleration, followed by a decrease (see the dashed curve in figure 1). Several interpretations have been offered for this phenomenon, such as the geometric effect of changes in finger tip curvature (Glimm *et al.* 2002), or strong vorticities at the tails of bubbles and spikes (Sohn 2011). Since the understanding of the dynamics of fingers in such a late stage is still progressing, we will not focus on the fingering growth in this possible re-acceleration stage.

2. Different behaviours between spikes and bubbles

It is well known that spikes and bubbles can exhibit qualitatively different behaviours. Spikes are more unstable than bubbles and consequently it is more difficult to predict the behaviour of spikes. Even among fingers of the same type, different fluid density ratios can lead to quantitatively different behaviours. The larger the density ratio, the more unstable is the finger. In addition, the spike in a system with an infinite density ratio shows completely different behaviour at late times from those in systems with finite density ratios. For RM instability, the former attains a constant velocity asymptotically while the latter decay with time; for RT instability, the former asymptotically grows with a constant acceleration while the latter grow with approximately constant velocities at the quasi-steady stage. These phenomena are

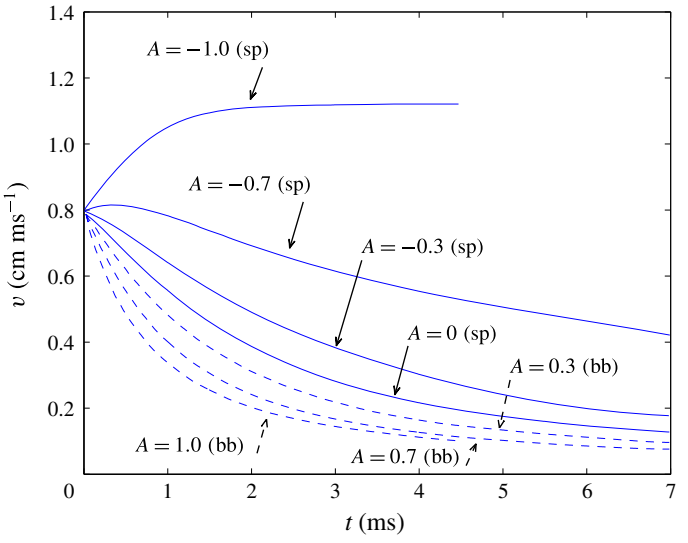

FIGURE 2. (Colour online) Spike (solid curves) and bubble (dashed curves) velocities at different Atwood numbers A from numerical simulations for RM instability (Sohn 2004). The initial conditions are $a_0 = 0.5$ cm and $v_0 = 0.8$ cm ms^{-1}, with $A = 0, \pm 0.3, \pm 0.7, \pm 1$.

well illustrated in figures 2–4 for RM instability, and in figure 5 for RT instability. In the captions of these figures, a_0 is the initial amplitude of the interface perturbation, v_0 is the initial velocity, k is the wavenumber, λ is the wavelength and g is the gravitational acceleration. The data for figures 2 and 5 are taken from Sohn (2004), in which the numerical simulations were performed with the vortex method (E & Hou 1990). The data for figure 3 are taken from Dimonte & Ramaprabhu (2010), and the data for figure 4 are taken from Alon *et al.* (1995). To describe density ratios, the Atwood number $A = (\rho_1 - \rho_2)/(\rho_1 + \rho_2)$ is commonly used, where ρ_i $(i = 1, 2)$ denotes the density of fluid i. Conventionally only a positive Atwood number is used for both spikes and bubbles of the same system, but in this paper we specifically use the positive Atwood number for bubbles, and its negative counterpart for spikes with the same density ratio. This allows us to express the results for both spikes and bubbles by the same function in the later analysis.

In this study, we investigate both spikes and bubbles in systems with all density ratios up through the quasi-steady stage, and report a very surprising result: by appropriately scaling the physical quantities, the main behaviours of growth rates of all fingers collapse onto a single curve. We call this curve 'universal' because it applies (1) among bubbles of different density ratios, (2) among spikes of different density ratios and (3) between bubbles and spikes of different density ratios.

The Layzer-type method has been extensively adapted in studying fingering instabilities. This method was initially introduced by Layzer (1955) to study the motion of a vacuum bubble in RT instability. The model was later extended by Hecht *et al.* (1994) to study bubbles in RM instability and by Mikaelian (1998) to study bubbles in cylindrical geometry. Zhang (1998) extended the model to the spike. All these studies are for systems with infinite density ratios. Goncharov (2002) generalized the method to finite density ratios. However, Mikaelian (2008) pointed out the problems in Goncharov's model: 'The failure for spikes becomes perhaps obvious for this model ... it is well known that spikes are 'sharper,' i.e. have larger $|\eta_2|$

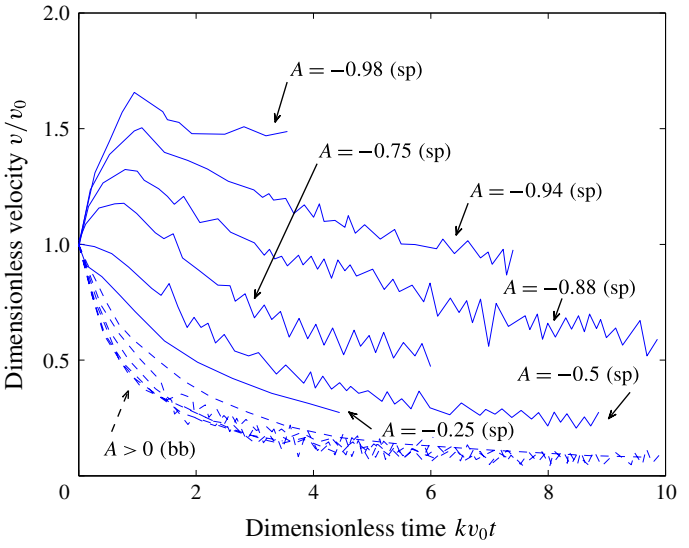

FIGURE 3. (Colour online) Spike (solid curves) and bubble (dashed curves) velocities at different Atwood numbers A from numerical simulations for RM instability (Dimonte & Ramaprabhu 2010). The initial condition is $a_0k = 0.125$, with $A = \pm0.25, \pm0.5, \pm0.75, \pm0.88, \pm0.94, \pm0.98$.

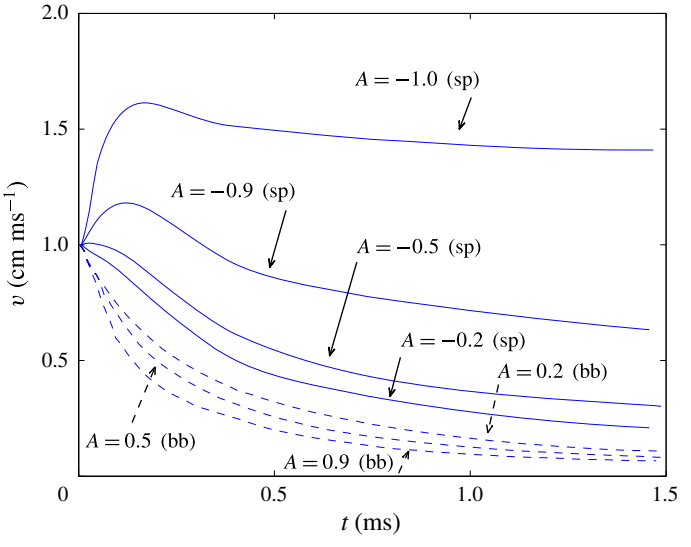

FIGURE 4. (Colour online) Spike (solid curves) and bubble (dashed curves) velocities at different Atwood numbers A from numerical simulations for RM instability (Alon *et al.* 1995). The initial conditions are $v_0 = 1$ cm ms^{-1} and $\lambda = 1$ cm, with $A = \pm0.2, \pm0.5, \pm0.9, -1$.

than bubbles, especially at large A. (Goncharov's) equation (4) is independent of A and clearly predicts the wrong curvature for Goncharov's spikes.' Later Abarzhi *et al.* (2003) and Sohn (2003) obtained similar growth rates with different approaches,

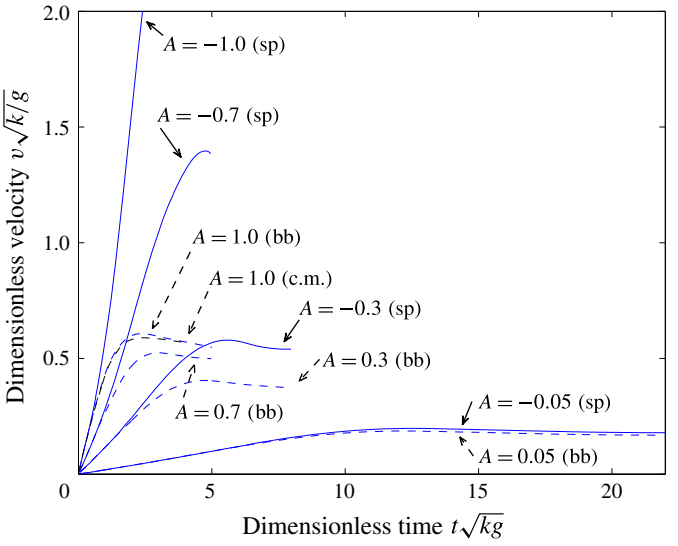

FIGURE 5. (Colour online) Spike (solid curves) and bubble (dashed curves) velocities at different Atwood numbers A from numerical simulations for RT instability. Blue curves: vortex model results from Sohn (2004), with $a_0k = 0.5$, $v_0 = 0$ and $A = \pm 0.05, \pm 0.3, \pm 0.7, \pm 1$. Black curve (labelled as c.m.): conformal mapping result from Menikoff & Zemach (1983), with the same initial conditions and $A = 1$.

however only for bubbles. Mikaelian (2003) proposed an analytic model for the evolution of the bubble amplitude from the linear to the nonlinear regime. From these works, we observe a list of characteristics that the finger curvature possesses:

(1) for infinite density ratio, the bubble curvature asymptotically tends to one-sixth of the wavenumber (Hecht *et al.* 1994; Mikaelian 1998; Zhang 1998; Goncharov 2002; Abarzhi *et al.* 2003; Sohn 2003);
(2) for infinite density ratio, the spike curvature asymptotically tends to infinity (Zhang 1998);
(3) the bubble curvature in the quasi-steady stage is insensitive to the density ratio (Sohn 2004).

Based on these properties we will deduce the finger growth rate for a system with any density ratio and show the universality of all fingers at late times, but before the possible re-acceleration stage.

3. Theoretical formulation

We consider incompressible, inviscid and irrotational fluids with arbitrary density ratio in two dimensions, whose governing equations (Layzer 1955) are

$$\nabla^2\phi_i(t, x, z) = 0, \tag{3.1}$$

$$\frac{\partial\eta}{\partial t} - \frac{\partial\phi_i}{\partial x}\frac{\partial\eta}{\partial x} + \frac{\partial\phi_i}{\partial z} = 0, \quad \text{at } z = \eta, \tag{3.2}$$

$$\sum_{i=1}^{2}(-1)^i\rho_i\left(-g\eta + \frac{\partial\phi_i}{\partial t} - \frac{1}{2}\left[\left(\frac{\partial\phi_i}{\partial x}\right)^2 + \left(\frac{\partial\phi_i}{\partial z}\right)^2\right]\right) = f(t), \quad \text{at } z = \eta. \tag{3.3}$$

Here $z=\eta(t,x)$ is the vertical position of the interface at time t, g is the gravitational acceleration, ϕ_i is the velocity potential, ρ_i is the fluid density, subscript i $(i=1,2)$ denotes the upper fluid and lower fluid, respectively, and $f(t)$ is an arbitrary function that depends only on time t.

In our configuration, a signed Atwood number is used to describe the density ratio. To elaborate, when studying bubbles, we consider the heavy fluid is on top of the light fluid with the acceleration pointing downwards. Therefore, the Atwood number $A=(\rho_1-\rho_2)/(\rho_1+\rho_2)>0$ and $g>0$ for bubbles. When studying spikes, we consider the light fluid is on top of the heavy fluid with the acceleration pointing upwards. Therefore, $A<0$ and $g<0$ for spikes. This setting allows us to consider only the case of the finger penetrating from the lower fluid into the upper fluid for both finger types (bubbles and spikes).

The shape of a finger tip (bubble or spike) is approximated as a parabola, $\eta(t,x)=z_0(t)+\xi(t)kx^2$. Here $z_0(t)$ and $\xi(t)$ are the vertical position and the curvature of the finger tip, respectively. In our configuration, the curvature is always non-positive, i.e. $\xi\leqslant 0$.

In theory, the velocity potential in phase 1 can be expressed in a series such as $\phi_1=\sum_{j=1}^{\infty}a_1^{(j)}(t)\cos(jkx)\mathrm{e}^{-jkz}=a_1^{(1)}(t)\cos(kx)\mathrm{e}^{-kz}+\sum_{j=2}^{\infty}a_1^{(j)}(t)\cos(jkx)\mathrm{e}^{-jkz}$. This usual standard perturbation expansion with modes k, $2k$, $3k$, ... is good for early-time behaviour, but not suitable for late-time approximation, since it is a divergent series for large times. Since our study focuses on the late-time behaviour of single-mode RT and RM instabilities, an approach that captures the dominant behaviour of fingers at late times is needed. The works in Layzer (1955), Hecht *et al.* (1994), Mikaelian (1998) and Zhang (1998) showed that, for $A=1$, modelling the system with only the primary mode k is sufficient to obtain a good approximation. However, as pointed out by Mikaelian (2008), for a system with $|A|\neq 1$, still modelling the system with only one mode had led to incorrect predictions for the asymptotic curvature. Thus, it is necessary to model the collective behaviour of all modes beyond the primary mode k. In our model, the first term $a_1^{(1)}(t)\cos(kx)\mathrm{e}^{-kz}$, abbreviated as $a_1(t)\cos(kx)\mathrm{e}^{-kz}$, represents the dominant behaviour of the finger, and we approximate the collective behaviour of all remaining terms $\sum_{j=2}^{\infty}a_1^{(j)}(t)\cos(jkx)\mathrm{e}^{-jkz}$ by $b_1(t)\cos(c(t)kx)\mathrm{e}^{-c(t)kz}$. Note that in our approximation the coefficient $c(t)$ depends on the Atwood number A, which is different from other approximations. Most approximations assume that the finger can be well expressed by the first few terms of the series $\sum_{j=1}^{n}a^{(j)}(t)\cos(jkx)\mathrm{e}^{-jkz}$, and each frequency is proportional to k and independent of A. Since we use an effective mode to represent the collective behaviour of all remaining modes $j=2,3,\ldots,$ and the coefficients of these modes depend on A, it follows that $c(t)$ in our approximation must also depend on A. We comment that $c(t)k$ is not an approximation for only the first few terms in the expansion, and it is not for the whole interface. It is a local approximation for the collective behaviour of all remaining modes near the finger tip. Although the same functional form $c(t,A,g)$ is used for both bubbles and spikes, in our signed Atwood number notation, namely, $A>0$, $g>0$ for bubbles and $A<0$, $g<0$ for spikes, we have $c_{bb}=c(t,|A|,|g|)$ and $c_{sp}=c(t,-|A|,-|g|)$. Therefore, the value of c_{bb} is different from that of c_{sp} in a system with a given density ratio. The velocity potential in phase 2 is approximated in a similar way. Therefore, we write the velocity potentials in the following form:

$$\phi_i(t,x,z)=a_i(t)\cos(kx)\mathrm{e}^{(-1)^i kz}+b_i(t)\cos(c(t)kx)\mathrm{e}^{(-1)^i c(t)kz},\quad i=1,2. \tag{3.4}$$

We comment that $a_i(t)$, $b_i(t)$, $c(t)$, $z_0(t)$ and $\xi(t)$ are also functions of A and g. For conciseness, we do not display them explicitly.

By substituting expression (3.4) into (3.2) and expanding the resulting equations through the order of x^2, we obtain:

$$\frac{\mathrm{d}z_0}{\mathrm{d}t} + (-1)^i k(a_i\,\mathrm{e}^{(-1)^i k z_0} + b_i\,c\,\mathrm{e}^{(-1)^i c\,k z_0}) = 0, \tag{3.5}$$

$$2\,\frac{\mathrm{d}\xi}{\mathrm{d}t} + 6k^2\xi\,(a_i\,\mathrm{e}^{(-1)^i k z_0} + b_i\,c^2\,\mathrm{e}^{(-1)^i c\,k z_0}) - (-1)^i k^2(a_i\,\mathrm{e}^{(-1)^i k z_0} + b_i\,c^3\,\mathrm{e}^{(-1)^i c\,k z_0}) = 0, \quad i = 1, 2. \tag{3.6}$$

One can solve for a_i and b_i explicitly from (3.5) and (3.6). After substituting the resulting expressions into (3.3), one can obtain an ordinary differential equation for the term proportional to x^2:

$$F_1\left[16\left(\frac{\mathrm{d}\xi}{\mathrm{d}t}\right)^2 - 10ckv\frac{\mathrm{d}\xi}{\mathrm{d}t} + c^2k^2v^2\right] + 2F_2\frac{\mathrm{d}\xi}{\mathrm{d}t}\frac{\mathrm{d}c}{\mathrm{d}t} + F_3kv\frac{\mathrm{d}c}{\mathrm{d}t} + F_4\left(2F_4kAg\xi - 2F_5\frac{\mathrm{d}^2\xi}{\mathrm{d}t^2} + F_6k\frac{\mathrm{d}v}{\mathrm{d}t}\right) = 0. \tag{3.7}$$

Here $v = \mathrm{d}z_0/\mathrm{d}t$ is the velocity of the finger tip, and

$$F_1 = A(c+1)^2 - 12\,\xi(c+1) + 36A\,\xi^2, \tag{3.8}$$

$$F_2 = (c+1)^2 - 12A\xi(c+1) + 36\,\xi^2, \tag{3.9}$$

$$F_3 = (c+1)^2 + 6A\,\xi(c^2-1) - 36\,\xi^2(2c+1) + 216A\,\xi^3, \tag{3.10}$$

$$F_4 = (c+1)^2 - 36\,\xi^2, \tag{3.11}$$

$$F_5 = c + 1 - 6A\,\xi, \tag{3.12}$$

$$F_6 = c^2 + c + 2A\,\xi(c^2 - c + 1) - 72A\,\xi^3. \tag{3.13}$$

The results from numerical simulations (Tryggvason 1988; Sohn 2004) and from theoretical analysis (Alon *et al.* 1995; Goncharov 2002) showed that, in the quasi-steady state, spikes have approximately constant velocities in RT instability with finite density ratios. Only in an infinite density ratio system, i.e. $A = -1$, does the spike approach free fall asymptotically. Therefore, we will consider the fingers with $A \in (-1, 1]$ in our analysis. If a theoretical model is consistent, one would expect that its solution should have the property that, as $A \to -1$, it approaches the behaviour of spikes in an infinite density ratio system. As we will see later, our solution indeed has this important consistency property.

We now examine the velocity of the finger in the quasi-steady stage. It has been shown that both the velocity and the curvature of the finger tip are insensitive to time in this stage (Glimm *et al.* 2002; Sohn 2004), namely, $\mathrm{d}v/\mathrm{d}t = 0$, $\mathrm{d}\xi/\mathrm{d}t = 0$ and $\mathrm{d}c/\mathrm{d}t = 0$. From this property, we obtain an equation from (3.7) for RT instability in the quasi-steady stage:

$$v_{qs}^2 = -\frac{2Ag\xi_{qs}\,(c_{qs}+1+6\,\xi_{qs})^2(c_{qs}+1-6\,\xi_{qs})^2}{kc_{qs}^2[(36\xi_{qs}^2 + (c_{qs}+1)^2)(1+A) - (c_{qs}+1+6\,\xi_{qs})^2]}, \tag{3.14}$$

where the constants v_{qs} and ξ_{qs} stand for the quasi-steady velocity and the quasi-steady curvature, respectively. The right-hand side of (3.14) must be non-negative for all

values of A. In this equation, A and g share the same sign, and ξ_{qs} is always non-positive. Therefore, to maintain a non-negative v_{qs}^2 it is required that

$$(36\xi_{qs}^2 + (c_{qs}+1)^2)(1+A) - (c_{qs}+1+6\,\xi_{qs})^2 \geqslant 0, \quad \text{for all } A \in (-1,\,1], \tag{3.15}$$

which is equivalent to

$$A\,(36+q^2) - 12q \geqslant 0, \quad \text{for all } A \in (-1,\,1], \tag{3.16}$$

where $q = (c_{qs}+1)/\xi_{qs}$. In the case of spikes, i.e. when $A<0$, the solution of (3.16) is

$$\frac{6}{A}(1+\sqrt{1-A^2}) \leqslant q \leqslant \frac{6}{A}(1-\sqrt{1-A^2}). \tag{3.17}$$

In particular, (3.17) must hold in the neighbourhood of $A=-1$, which gives

$$q = -6 + o(1), \tag{3.18}$$

namely, $c_{qs}/\xi_{qs} = -6 - 1/\xi_{qs} + o(1) = -6 + o(1)$, since $1/\xi_{qs} = o(1)$ by property (2) at the end of § 2. Therefore, we obtain $c_{qs} = -6\,\xi_{qs}(1+o(1))$ in the neighbourhood of $A=-1$. To the leading-order approximation, we will approximate c_{qs} by $-6\xi_{qs}$. We now determine the behaviour of ξ_{qs} near $A=-1$. After approximating c_{qs} by $-6\xi_{qs}$, a condition for ξ_{qs} can be deduced from (3.15):

$$72\zeta^2 - 12\zeta\sqrt{1+A} + (1+A) \geqslant 1, \tag{3.19}$$

where $\zeta = \xi_{qs}\sqrt{1+A}$. In the neighbourhood of $A=-1$, the left-hand side of (3.19) will be determined by the leading term:

$$72\zeta^2 \geqslant 1. \tag{3.20}$$

The equality in (3.19) holds for the case in which the expression inside the square bracket in the denominator of (3.14) tends to zero. This corresponds to the largest growth rate for the spike near $A=-1$. Therefore, to obtain the most unstable growth rate, we require $72\zeta^2 = 1$, i.e.

$$\xi_{qs} = -\frac{\sqrt{2}}{12\sqrt{(1+A)}}, \quad \text{as } A \to -1. \tag{3.21}$$

Equation (3.21) suggests that $\xi_{qs}(A)$ should have a Laurent series in terms of $\sqrt{1+A}$, and we will keep only the three leading terms, namely,

$$\xi_{qs}(A) = -\frac{\sqrt{2}}{12}(1+A)^{-1/2} + d_0 + d_1(1+A)^{1/2}. \tag{3.22}$$

Property (1) of § 2 requires, when $A=1$, that $\xi_{qs}(1) = -1/6$, which means

$$-\tfrac{1}{12} + d_0 + \sqrt{2}d_1 = -\tfrac{1}{6}. \tag{3.23}$$

To capture property (3), we take $(\mathrm{d}\xi_{qs}/\mathrm{d}A)|_{A=1} = 0$, which provides another equation:

$$\frac{1}{48} + \frac{\sqrt{2}}{4}d_1 = 0. \tag{3.24}$$

Equations (3.23) and (3.24) give $d_0 = 0$ and $d_1 = -1/(12\sqrt{2})$. Thus, we obtain the quasi-steady curvature

$$\xi_{qs}(A) = -\frac{1}{12}\left(\sqrt{\frac{2}{1+A}} + \sqrt{\frac{1+A}{2}}\right) = -\frac{3+A}{12\sqrt{2(1+A)}} \tag{3.25}$$

from (3.22), and the quasi-steady velocity

$$v_{qs}(A) = \left(\frac{Ag}{3k}\frac{8}{(1+A)(3+A)}\frac{[3+A+\sqrt{2}\,(1+A)^{1/2}]^2}{[4(3+A)+\sqrt{2}\,(9+A)(1+A)^{1/2}]}\right)^{1/2} \tag{3.26}$$

from (3.14) for RT instability. We comment that the result given by (3.26) is valid for both spikes ($A < 0,\ \ g < 0$) and bubbles ($A > 0,\ \ g > 0$).

As given by (3.26) v_{qs} is the velocity at the quasi-steady stage. The leading-order contribution at early times is just the initial condition v_0. It is desirable to have an asymptotic matched solution for both early and quasi-steady stages. To achieve this, we approximate $\xi(t)$ by ξ_{qs} and $c(t)$ by $-6\xi_{qs}$. This is motivated by the analytical results for $A = 1$ (Mikaelian 1998; Zhang 1998). Equations (4) and (7) in Zhang (1998) show that $\xi(t)$ approaches its asymptotic value much faster than $v(t)$ does: $\xi(t)$ approaches its asymptotic value at the rate of e^{-3kz_0}; $v(t)$ approaches its asymptotic value at the rate of $\mathrm{e}^{-[3kz_0-\ln(kz_0)]/2}$, which is much slower than e^{-3kz_0}. Therefore, it is reasonable to approximate $\xi(t)$ as a constant. Since, in our analysis, the asymptotic value of $c(t)$ is related to that of $\xi(t)$, it is reasonable to approximate $c(t)$ as a constant as well. Under these approximations, (3.7) becomes

$$\frac{\mathrm{d}v}{\mathrm{d}t} = -\alpha k(v^2 - v_{qs}^2), \tag{3.27}$$

where

$$\alpha = \frac{3}{4}\frac{(1+A)(3+A)}{[3+A+\sqrt{2}(1+A)^{1/2}]}\frac{[4(3+A)+\sqrt{2}\,(9+A)(1+A)^{1/2}]}{[(3+A)^2+2\sqrt{2}\,(3-A)(1+A)^{1/2}]}, \tag{3.28}$$

which is a function of the Atwood number A. Therefore, a matched solution for v can be obtained by integrating (3.27) from 0 to t.

4. Universality of fingers at all density ratios

For RM instability, we take the limit $g \to 0$ in (3.27) and obtain

$$\frac{\mathrm{d}v}{\mathrm{d}t} = -\alpha k v^2, \tag{4.1}$$

and the matched solution is

$$v = \frac{v_0}{1+\alpha k v_0 t}, \tag{4.2}$$

where v_0 denotes the initial velocity. When $A = 1$, the expression given by (4.2) recovers the results shown by Mikaelian (1998) and Buttler *et al.* (2012).

If we introduce the scaled dimensionless variables

$$u_{RM} = \frac{v}{v_0}, \quad \tau_{RM} = \alpha k v_0 t, \tag{4.3a,b}$$

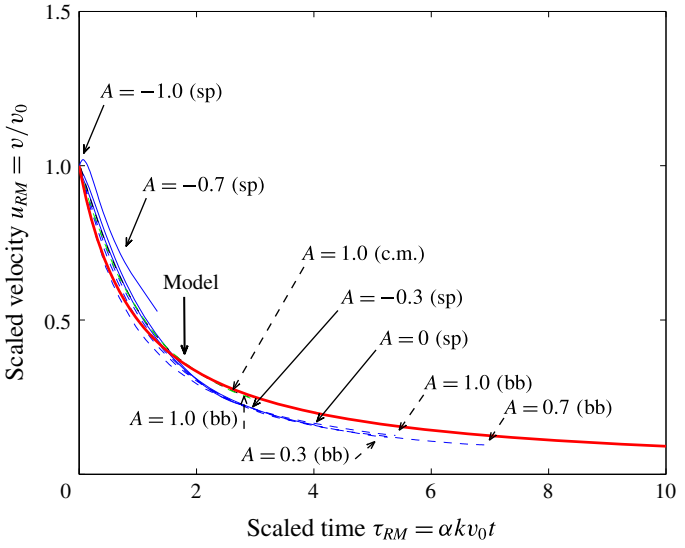

FIGURE 6. (Colour online) Comparison between universality curve given by (4.4) and scaled data from figure 2 for RM instability at different Atwood numbers. The solid curves are the scaled spike velocities, and the dashed curves are the scaled bubble velocities. Red curve: universality model prediction. Blue curves: vortex model results from Sohn (2004) with $a_0 = 0.5$ cm $v_0 = 0.8$ cm ms^{-1} and $A = 0, \pm 0.3, \pm 0.7, 1$. Black curve and green curve: $a_0 = 0$ and $v_0 = 0.5$ cm ms^{-1}, with $A = 1$. The black curve (labelled as c.m.) is the conformal mapping result from Menikoff & Zemach (1983), and the green curve is the vortex model result from Sohn (2004).

then (4.2) can be written as

$$u_{RM} = \frac{1}{1 + \tau_{RM}}. \tag{4.4}$$

It is completely unexpected that, despite the different behaviours among fingers with various Atwood numbers, and even the qualitative distinctions between spikes and bubbles, the growth rates of all finger tips, up through the quasi-steady stage, can be approximately described by a single equation in terms of the appropriately scaled dimensionless variables given by (4.3). This equation is independent of finger types and of the Atwood number. This means that, in terms of scaled variables, the dominant behaviours of the growth rates of all fingers (both spikes and bubbles) at all Atwood numbers follow a universal curve for systems governed by (3.1)–(3.3). Furthermore, the result of the bubble growth rate at any specific Atwood number can be used to predict (through scaling) not only the bubble growth rates at other Atwood numbers, but also the spike growth rates at all Atwood numbers. Similarly, one can also use the result of a spike to do such predictions. This implies that, to study the growth rates for both finger types and for all Atwood numbers, one only needs to study the behaviour of one finger at any Atwood number. This is particularly important and useful for numerical simulations and experiments, since it is highly time-consuming and also possibly expensive to perform studies for multiple Atwood numbers up through the nonlinear stage.

To verify our prediction on universality, we apply (4.3) to scale all the results from numerical simulations shown in figures 2–4, and compare the scaled results with our prediction given by (4.4). The comparison results are presented in figures 6–8. All

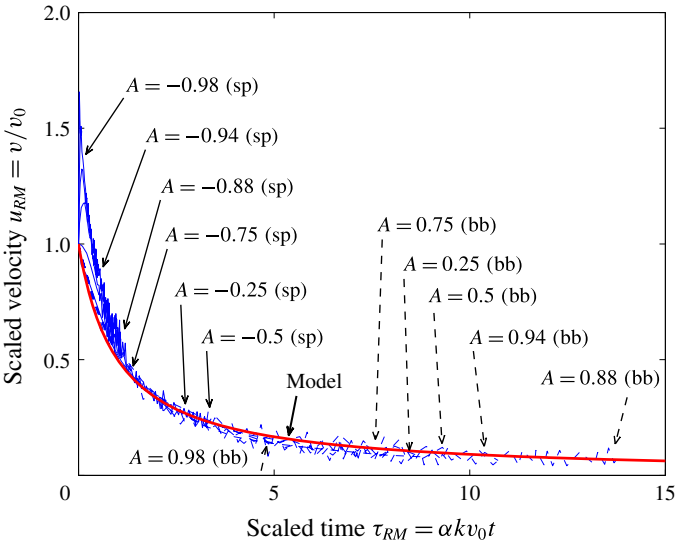

FIGURE 7. (Colour online) Comparison between universality curve given by (4.4) and scaled data from figure 3 for RM instability at different Atwood numbers. The solid curves are the scaled spike velocities, and the dashed curves are the scaled bubble velocities. Red curve: universality model prediction. Blue curves: numerical results (FLASH) from Dimonte & Ramaprabhu (2010), with $a_0 k = 0.125$ and $A = \pm 0.25, \pm 0.5, \pm 0.75, \pm 0.88, \pm 0.94, \pm 0.98$.

results from three sets of data show that the scaled data are in good agreement with our universality curve. The scaled results also show that, in terms of scaled time, longer simulations are needed for spikes with large Atwood numbers to reach the quasi-steady stage. This may not be obvious in the original unscaled data.

The scaling technique can also be applied to RT instability. By expressing (3.27) in terms of the scaled dimensionless variables

$$u_{RT} = \frac{v}{v_{qs}} \quad \text{and} \quad \tau_{RT} = \alpha k v_{qs} t, \tag{4.5a,b}$$

we obtain a universal curve for the scaled velocity in RT instability:

$$u_{RT} = \frac{1 - r\,\mathrm{e}^{-2\tau_{RT}}}{1 + r\,\mathrm{e}^{-2\tau_{RT}}}, \tag{4.6}$$

where $r = [1 - u_{RT}(0)]/[1 + u_{RT}(0)]$.

Figure 9, the scaled version of figure 5, also shows the similarity and the universality between the growth rate of spikes and that of bubbles at different Atwood numbers for RT instability. Despite the different developments in the early stage, the scaled physical quantities for all fingers are gradually approaching the same universality curve. The agreement between the theoretical prediction and the scaled numerical data for RT instability shown in figure 9 is not as good as those for RM instability shown in figures 6–8. This is due to several reasons. (1) The fingers in RT instability are driven by gravity, and therefore are more unstable than those in RM instability. Thus, it is much harder to carry out the simulations for

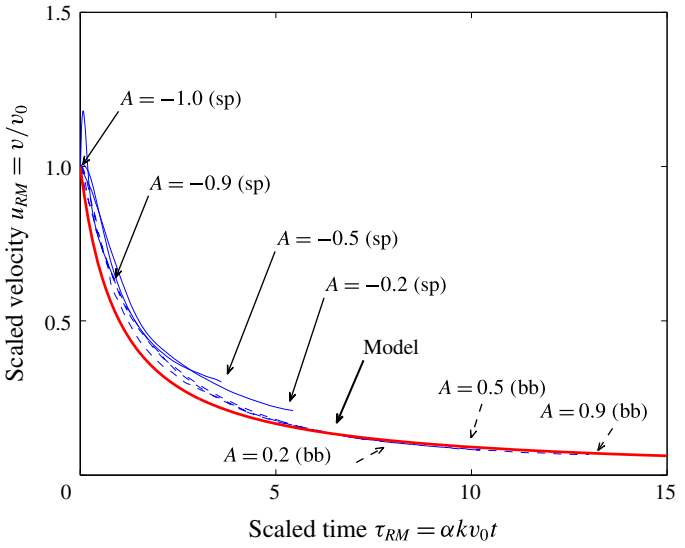

FIGURE 8. (Colour online) Comparison between universality curve given by (4.4) and scaled data from figure 4 for RM instability at different Atwood numbers. The solid curves are the scaled spike velocities, and the dashed curves are the scaled bubble velocities. Red curve: universality model prediction. Blue curves: numerical results (LEEOR2D) from Alon *et al.* (1995), with $v_0 = 1$ cm ms^{-1}, $\lambda = 1$ cm and $A = \pm 0.2, \pm 0.5, \pm 0.9$.

RT instability to the asymptotic regime. They need a larger computational domain and longer computing time. Owing to these difficulties, in terms of scaled time, the numerical simulations for RT instability were actually terminated earlier than those for RM instability. (2) Since in terms of scaled time the simulations for RT instability are shorter than those for RM instability, they contain more transient effects, which are not included in our model. (3) In the numerical simulations presented by Sohn (2004), a numerical desingularization parameter is introduced to avoid singularities in computation, which reduces the growth rates. Therefore, the numerical data are consistently below our theoretical prediction. For the same reason, the numerical results shown in figure 6 are also slightly lower than our theoretical prediction. In particular, figure 9 shows that the simulation for the spike at $A = -0.7$ ends too soon and has not approached the quasi-steady stage yet. Therefore, we call for further numerical studies of RT instability in late times, especially for spikes with large Atwood numbers.

5. Discussion

Our derivation is based on $A \in (-1, 1]$. However, one would expect that a consistent theoretical model should have the property that in the limit $A \to -1$ the solution of the model approaches the known behaviour for $A = -1$, namely, it should recover the behaviour of spikes in an infinite density ratio system. We now examine this limit. In the limit $A \to -1$, α given by (3.28) tends to 0. Consequently, the scaled times τ_{RM} and τ_{RT} given by (4.3) and (4.5) tend to 0 as well. This shows that, for both RM and RT instabilities, the asymptotic behaviour of spikes in an infinite density ratio system corresponds to the point $\tau = 0$ on our universality curve. For RM instability, since $\tau_{RM} \to 0$, (4.4) becomes $u_{RM} = 1$, namely, $v = v_\infty = v_0$. This agrees with the

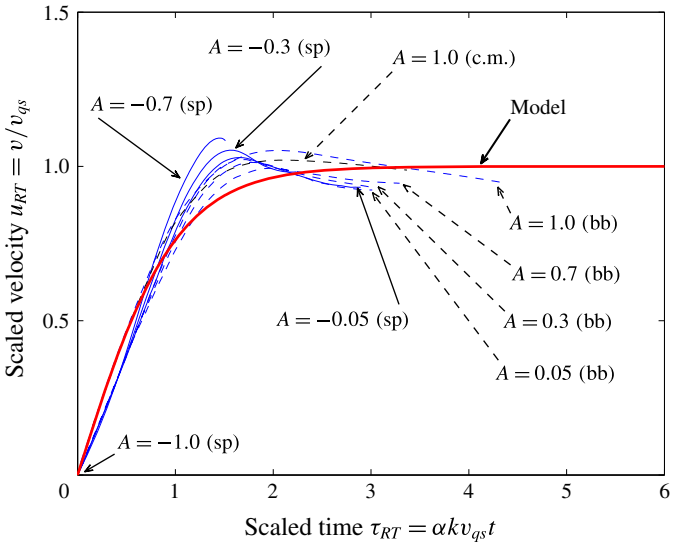

FIGURE 9. (Colour online) Comparison between universality curve given by (4.6) and scaled data from figure 5 for RT instability at different Atwood numbers. The solid curves are the scaled spike velocities, and the dashed curves are the scaled bubble velocities. Red curve: universality model prediction. Blue curves: vortex model results from Sohn (2004), with $a_0 k = 0.5$, $v_0 = 0$ and $A = \pm 0.05, \pm 0.3, \pm 0.7, 1$. Black curve (labelled as c.m.): conformal mapping result from Menikoff & Zemach (1983), with the same initial conditions and $A = 1$.

prediction of $v_\infty = v_0[(6\xi_0 + 3)/(6\xi_0 + 1)]^{1/2}$ given by Zhang (1998), since in our analysis $\xi_0 = \xi_\infty = \infty$. For RT instability, by taking the limit $A \to -1$ in (3.27), we obtain $\mathrm{d}u_{RT}/\mathrm{d}\tau = 1$, namely, $\mathrm{d}v/\mathrm{d}t = \mathrm{d}v/\mathrm{d}t|_{t=\infty} = |g|$ in terms of unscaled variables. This expression also agrees with the prediction given by Zhang (1998), and recovers the free-fall behaviour of RT spikes in an infinite density ratio system. This shows that our derivation based on $A \in (-1, 1]$ indeed recovers the known results for $A = -1$. Therefore, our theory is for all density ratios.

For an initial interface randomly perturbed by many different modes, a turbulent mixing zone forms at late times. It has been shown that the size of the turbulent mixing zone has certain important scaling behaviour at late times (Alon *et al.* 1995; Dimonte & Schneider 2000; Poujade & Peybernes 2010; Thornber *et al.* 2010; Tritschler *et al.* 2014). It is known that the dynamics of a mixing zone is governed by the growth of each individual mode and by the interaction between adjacent bubbles. In this paper the universal scaling behaviour for single-mode RT and RM instabilities is shown. If one can further establish a scaling behaviour for bubble interaction, then potentially one could provide a better understanding of the scaling behaviour of turbulent mixing zones.

Acknowledgement

The work of Q.Z. was supported by the Research Grants Council of the Hong Kong Special Administrative Region, China (project CityU 11303714).

REFERENCES

ABARZHI, S. I., GLIMM, J. & LIN, A.-D. 2003 Dynamics of two-dimensional Rayleigh–Taylor bubbles for fluids with a finite density contrast. *Phys. Fluids* **15** (8), 2190–2197.

ALON, U., HECHT, J., OFER, D. & SHVARTS, D. 1995 Power laws and similarity of Rayleigh–Taylor and Richtmyer–Meshkov mixing fronts at all density ratios. *Phys. Rev. Lett.* **74** (4), 534–537.

BROUILLETTE, M. 2002 The Richtmyer–Meshkov instability. *Annu. Rev. Fluid Mech.* **34** (1), 445–468.

BUTTLER, W. T., ORÓ, D. M., PRESTON, D. L., MIKAELIAN, K. O., CHERNE, F. J., HIXSON, R. S., MARIAM, F. G., MORRIS, C., STONE, J. B., TERRONES, G. & TUPA, D. 2012 Unstable Richtmyer–Meshkov growth of solid and liquid metals in vacuum. *J. Fluid Mech.* **703**, 60–84.

DIMONTE, G. & RAMAPRABHU, P. 2010 Simulations and model of the nonlinear Richtmyer–Meshkov instability. *Phys. Fluids* **22** (1), 014104.

DIMONTE, G. & SCHNEIDER, M. 2000 Density ratio dependence of Rayleigh–Taylor mixing for sustained and impulsive acceleration histories. *Phys. Fluids* **12** (2), 304–321.

E, W. & HOU, T. Y. 1990 Homogenization and convergence of the vortex method for 2-D Euler equations with oscillatory vorticity fields. *Commun. Pure Appl. Maths* **43** (7), 821–855.

GLIMM, J., LI, X.-L. & LIN, A.-D. 2002 Nonuniform approach to terminal velocity for single mode Rayleigh–Taylor instability. *Acta Math. Appl. Sinica* **18** (1), 1–8.

GONCHAROV, V. 2002 Analytical model of nonlinear, single-mode, classical Rayleigh–Taylor instability at arbitrary Atwood numbers. *Phys. Rev. Lett.* **88** (13), 134502.

HECHT, J., ALON, U. & SHVARTS, D. 1994 Potential flow models of Rayleigh–Taylor and Richtmyer–Meshkov bubble fronts. *Phys. Fluids* **6**, 4019–4030.

LAYZER, D. 1955 On the instability of superposed fluids in a gravitational field. *Astrophys. J.* **122**, 1–12.

MENIKOFF, R. & ZEMACH, C. 1983 Rayleigh–Taylor instability and the use of conformal maps for ideal fluid flow. *J. Comput. Phys.* **51** (1), 28–64.

MESHKOV, E. E. 1969 Instability of the interface of two gases accelerated by a shock wave. *Fluid Dyn.* **4**, 101–104.

MIKAELIAN, K. O. 1998 Analytic approach to nonlinear Rayleigh–Taylor and Richtmyer–Meshkov instabilities. *Phys. Rev. Lett.* **80** (3), 508–511.

MIKAELIAN, K. O. 2003 Explicit expressions for the evolution of single-mode Rayleigh–Taylor and Richtmyer–Meshkov instabilities at arbitrary Atwood numbers. *Phys. Rev.* E **67** (2), 026319.

MIKAELIAN, K. O. 2008 Limitations and failures of the Layzer model for hydrodynamic instabilities. *Phys. Rev.* E **78** (1), 015303.

POUJADE, O. & PEYBERNES, M. 2010 Growth rate of Rayleigh–Taylor turbulent mixing layers with the foliation approach. *Phys. Rev.* E **81** (1), 016316.

RAYLEIGH, LORD 1883 Investigation of the character of the equilibrium of an incompressible heavy fluid of variable density. *Proc. Lond. Math. Soc.* **14**, 170–177.

RICHTMYER, R. D. 1960 Taylor instability in shock acceleration of compressible fluids. *Commun. Pure Appl. Maths* **13** (2), 297–319.

SHARP, D. H. 1984 An overview of Rayleigh–Taylor instability. *Physica* D **12** (1), 3–18.

SOHN, S.-I. 2003 Simple potential-flow model of Rayleigh–Taylor and Richtmyer–Meshkov instabilities for all density ratios. *Phys. Rev.* E **67** (2), 026301.

SOHN, S.-I. 2004 Vortex model and simulations for Rayleigh–Taylor and Richtmyer–Meshkov instabilities. *Phys. Rev.* E **69** (3), 036703.

SOHN, S.-I. 2011 Late-time vortex dynamics of Rayleigh–Taylor instability. *J. Phys. Soc. Japan* **80** (8), 084401.

TAYLOR, G. 1950 The instability of liquid surfaces when accelerated in a direction perpendicular to their planes. I. *Proc. R. Soc. Lond.* A **201** (1065), 192–196.

THORNBER, B., DRIKAKIS, D., YOUNGS, D. L. & WILLIAMS, R. J. R. 2010 The influence of initial conditions on turbulent mixing due to Richtmyer–Meshkov instability. *J. Fluid Mech.* **654**, 99–139.

TRITSCHLER, V. K., OLSON, B. J., LELE, S. K., HICKEL, S., HU, X. Y. & ADAMS, N. A. 2014 On the Richtmyer–Meshkov instability evolving from a deterministic multimode planar interface. *J. Fluid Mech.* **755**, 429–462.

TRYGGVASON, G. 1988 Numerical simulations of the Rayleigh–Taylor instability. *J. Comput. Phys.* **75** (2), 253–282.

ZHANG, Q. 1998 Analytical solutions of Layzer-type approach to unstable interfacial fluid mixing. *Phys. Rev. Lett.* **81** (16), 3391–3394.